Molecular Catalysis 488 (2020) 110901

Contents lists available at ScienceDirect

Molecular Catalysis

journal homepage: www.elsevier.com/locate/mcat

Simultaneous catalytic oxidation of nitric oxide and elemental mercury by single-atom Pd/g-C_3N_4 catalyst: A DFT study

Xiaoshuo Liu[a,b], Zhengyang Gao[a,*], Hanyu Huang[a], Ge Yan[a], Tianfang Huang[b], Cong Chen[b], Weijie Yang[a], Xun-Lei Ding[c,*]

[a] School of Energy and Power Engineering, North China Electric Power University, Baoding, 071003, China
[b] Key Laboratory of Energy Thermal Conversion and Control of Ministry of Education, School of Energy and Environment, Southeast University, Nanjing, 210096, China
[c] School of Mathematics and Physics, North China Electric Power University, Beijing, 102206, China

ARTICLE INFO

Keywords:
Single-atom palladium catalyst
Graphitic carbon nitride
Hg^0oxidation
NO oxidation
Thermodynamic and kinetic analysis

ABSTRACT

To realize simultaneous removal of pollutants released from coal-fired power plants, we carried out a theoretical study on catalytic oxidation of NO and Hg^0 on the surface of single-atom Pd/g-C_3N_4 catalyst (Pd_{sac}/g-C_3N_4), because after NO and Hg^0 are converted to NO_2 and Hg^{2+}, products can be well absorbed in WFGD by using higher water solubility. Detailed reaction patterns in the mechanisms of Eley-Rideal (E-R), Langmuir-Hinshelwood (L-H), and termolecular Eley-Rideal (TER) were involved in this calculation. We revealed characteristics of catalytic reactions in thermodynamics and kinetics, and it was found most reactions were favorable in thermodynamics, and part reaction paths can take place spontaneously and irreversibly. Kinetics analysis evidenced the chemical reaction rates were all very fast because of short half-lives of reactants and large reaction rate constants. Fitted Arrhenius formula suggested the lowest activation energies of NO and Hg^0 oxidation were just 0.46 eV and 1.81 eV, and therefore we speculated that Pd_{sac}/g-C_3N_4 catalyst should be a potential catalyst for catalytic oxidation of NO and Hg^0.

1. Introduction

Nitrogen oxides (NO_x), and mercury species (Hg) have been considered to be important compositions of air pollution, and drawn global concern due to their considerable contribution to depletion of ozone, formation of acid rain, occurrence of photochemical smog, and persistent damages to human's health [1,2], therefore demonstrating huge urgency on their abatement.

Coal-fired power plants are observed as one of the primary anthropogenic emission sources of these pollutions [3,4], and even with the equipment of air pollution control devices for coal-fired power plants, the total amounts of Hg, NO_x, and SO_2 released from power industry in China of 2017 year were still up to 468.87 ton [5], 1.14 million ton [6], and 1.20 million ton [6], respectively. To control pollution emission, coal-burning power stations tend to equip with complex air pollution control devices including selective catalytic reduction device via ammonia injection (SCR-NH_3) to de-NO_x [7–9], activated carbon injection method (ACI) to de-Hg^0 [10–12] and wet flue gas desulfurization (WFGD) device to de-SO_2 [13,14]. Although these technologies have been widely utilized in coal-fired power plants, it remains many serious and ineligible disadvantages. In detail, for ACI method to de-Hg^0, the main issue is the high cost of carbonaceous sorbents [15]; for SCR-NH_3 equipment to de-NO_x, disadvantages mainly include catalyst poisoning [16], poor catalytic rate at low temperature [17], and catalyst massive attrited consumption at high temperature [17]. More seriously, NH_3 used in SCR-NH_3 method is a kind of hazardous gas, and leakage of NH_3 can not only hurt human's vision, skins, and respiratory systems, but also can generate ammonium salt which may block the heat exchange tubes, bringing about security risks [3]. In addition, traditional SCR catalyst such as V_2O_5-MoO_3/TiO_2 and WO_3/TiO_2 are poisonous materials, and after several years of application, these catalysts would become chemical waste causing secondary pollution for environment [18,19]. Therefore, it is very valuable and imperative to explore new technology to control NO_x and Hg^0 emission from coal-fired power plants.

Simultaneous catalytic oxidation of NO and Hg^0 has been seen as a potential substitute for traditional ways [20–25], and as a kind of clean gas, oxygen [26,27] instead of toxic chlorine [28,29], hydrogen chloride [20], hydrogen bromide [30], and ozone [31,32], could be seen as a no-pollution oxidant for catalytic oxidation of NO and Hg^0. After NO and Hg^0 molecules are converted to NO_2 and HgO molecules by O_2, the generated NO_2 and HgO can be conveniently removed

* Corresponding authors.
E-mail addresses: gaozhyan@163.com (Z. Gao), dingxl@ncepu.edu.cn (X.-L. Ding).

https://doi.org/10.1016/j.mcat.2020.110901
Received 19 December 2019; Received in revised form 7 March 2020; Accepted 18 March 2020
Available online 11 April 2020

through wet flue gas desulfurization (WFGD) device owing to good water solubility of NO_2 and Hg^{2+} [33]. Besides, catalytic oxidation of Hg^0 can also improve removal capacity of unburned char for mercury species due to increased adsorption energy, from −0.3 eV [34] (Hg^0) to −3.21 eV [35] (HgO). However, it is extremely tough for elemental mercury (Hg^0) and NO molecules to be oxidized to Hg^{2+} and NO_2 in flue gas. It is widely known that the homogeneous oxidation efficiency of Hg^0 with O_2 in flue gas tends to be low (nearly zero) [36], and even if parts of SCR catalysts such as MnO_x-CeO_2/TiO_2 [37,38] have good performance on Hg^0 catalytic oxidation, SCR catalysts can barely achieve simultaneous removal of NO_x without injection of hazardous NH_3. In addition, NO molecules can hardly be oxidized in boilers as manifested by NO still takes up the main proportion of NO_x in flue gas [39]. Therefore, to realize wide application of NO catalytic oxidation and Hg^0 catalytic oxidation technology in the future, the key issue is to design and prepare compelling catalyst with low chemical reaction energy barrier for catalysis.

Noble metal catalysts were considered as primary choices for catalysis of small gases because of their compelling catalytic activity, and in particular Pd-contained catalysts were considered to be the one of the most attractive options for Hg^0 oxidation [40]. According to study of Hou et al. [41], the oxidation rate of elemental mercury by the surface of Pd-based catalyst can exceed 90 %, and in the light of report of Xu et al [42], graphene-supported Pd catalyst can also catalyze small gas such as CO molecule very well, with a relative low energy barrier of 0.29 eV, so it is natural for us to select Pd as the candidate for selection of catalyst in the usage of simultaneous oxidation of nitric oxide and elemental mercury.

The high cost of Pd metal has been a obvious shortcoming in its commercial application, but single-atom catalysts (SACs) can sharply reduce the usage amount of noble metal in catalysis. With the advantages of high activity, selectivity and atomic utilization rate, SACs have become a hotspot in the fields of catalysis science and chemical engineering [43–46]. Vorobyeva et al. [47] prepared g-C_3N_4 by calcination of cyanamide at the temperature over 820 K, and then succeed in anchoring single-atom dispersed Pd atoms on the hexagonal cavity of g-C_3N_4 substance by post-synthetic microwave irradiation assisted deposition, with the metal loading radio of 0.5 wt.% relative to the carriers. Considering the material synthesis method was well developed to simplicity, and single-atom Pd/g-C_3N_4 catalyst has shown great capacity for series chemical reactions, such as CO oxidation [48], CO_2 reduction [49] and O_2 activation [50], it is natural for us speculate this catalyst may hold outstanding performance on catalytic oxidation of NO and elemental mercury molecules.

In this work, we systematically studied the adsorption characteristics of reaction gas as well as chemical reaction paths in different reaction mechanisms, and performed comprehensive analysis using thermodynamics and reaction kinetics methods to talk about the feasibility of simultaneous catalytic oxidation of nitric oxide and elemental mercury on the surface of Pd_{sac}/g-C_3N_4 catalyst in flue gas. As we know, it is first time to propose simultaneous removal of Hg^0 and NO by multi-catalytic oxidation using SACs, and we hope our work can not only contribute to the further understanding of g-C_3N_4-based catalysts, but also provide important guidelines for pollution elimination from coal-fired power plants.

2. Computational methods

All calculations in this work were carried out using density functional theory (DFT), and the combination of Perdew-Burke-Ernzerhof (PBE) functional and projector augmented wave (PAW) potentials was utilized in the software of Vienna ab initio simulation package (VASP 5.4.1) [51]. It has widely convinced that the method of PBE-PAW is a great way for calculating the interaction between small-size gas molecules and solid surface [52–54]. Taking into consideration of atomic magnetism, the impact of spin polarization was added [55], and considering the effect of weak interaction, van der Waals dispersion correction (Grimme-D3) was involved in our calculations [56]. In the light of researches of others, a 2 × 2 × 1 g-C_3N_4 supercell was created [49,57], and a 15 Å vacuum layer was set up to avoid the effect of mirror interaction [58].

The cutoff energy of 500 eV was determined for the plane-wave basis set by corresponding test, taking both calculation accuracy and time cost into account, and detailed test data can be acquired in Fig. S1. In accordance with previous reports [59–61], the value of Gaussian smearing is determined as 0.05 eV in metal-carbon-nitrogen atoms systems, and a 3 × 3 × 1 Γ-centered k-point mesh grid is used for the calculation of structure relaxation, which has been proved to be rational and accurate by our test in Fig. S2 and others' previous study [62]. In detail, the threshold of structure relax was set at the level of 0.05 eV/Å, same as previous literature [62]. To get more accurate energy information, a 7 × 7 × 1 Γ-centered k-point mesh grid was adopted for electronic self-consistent field calculation, and the convergence precision was 1×10^{-5} eV.

To located transition states in reaction paths, we adopted a method of joint application of climbing-image nudged elastic band (Cl-NEB) [63,64] and improved dimer (IDM) [65], same as our previous works [66,67]. Cl-NEB method was utilized to roughly locate the geometry structures of transition states, at a 1 × 1 × 1 Γ-centered k-point mesh grid level and with the force convergence of 0.1 eV/Å, and then based on the rough structure, IDM method was used to acquire accurate structure of transition states at the 3 × 3 × 1 Γ-centered k-point mesh grid level with the force convergence of 0.05 eV/Å. In addition, to check the structure of transition states and to get thermodynamic energy, vibrational frequency calculations were performed, with finite displacement of ± 0.02 Å [68].

Adsorption energy (E_{ads}) was applied to describe the adsorption strength between catalyst surface and corresponding gases, and values of E_{ads} can be calculated by Eq. (1) [69,70].

$$E_{ads} = E_{sys} - E_{gas} - E_{cata} \quad (1)$$

Where E_{sys}, E_{gas}, and E_{cata} present the energy of total adsorption system, isolated free gases, and pure catalyst, respectively. In detail, if the value of E_{ads} is negative, it means this adsorption process is spontaneous, and when the absolute value of E_{ads} exceeds 0.5 eV, the adsorption would belong to stable chemical adsorption [71].

The oxidation energy barrier (E_{oxi}) of each step in reaction paths can be obtained from Eq. (2) [39]. It is worth noting that total energy barrier (E_{bar}) consists of oxidation energy barrier (E_{oxi}) and desorption energy barrier of products from catalyst (E_{dsp}), thus E_{bar} should be the largest value between E_{oxi} and E_{dsp}.

$$E_{oxi} = E_{TS} - E_{IS} \quad (2)$$

Where E_{IS} and E_{TS} mean the energy of adsorption initial states and transition states, respectively.

Thermodynamics analysis was carried out to explore the reaction equilibrium constants (K), and it was can be calculated from the Eq. (3) [72].

$$\Delta G = G_{FS} - G_{IS} = -RT \times LnK \quad (3)$$

Where G_{FS} and G_{IS} are the Gibbs free energy of finial state and initial state of each reaction path, respectively. In addition, the Gibbs free energy of gas and solid catalyst can be obtained via the Eqs. (4) and (5), respectively [73].

$$G_{gas}(T) = E_{ele} + ZPE + RT - TS \quad (4)$$

$$G_{solid}(T) = E_{ele} + ZPE - TS \quad (5)$$

Where E_{ele} is the electron energy of chemicals in ground-state; ZPE is the zero-point energy; R means the universal gas constant, 8.62×10^{-5} eV·mol^{-1}·k^{-1}; T is the Kelvin temperature; S is the entropy, and values of entropies were calculated by vibrational frequency analysis.

Kinetic analysis was carried out based on conventional transition

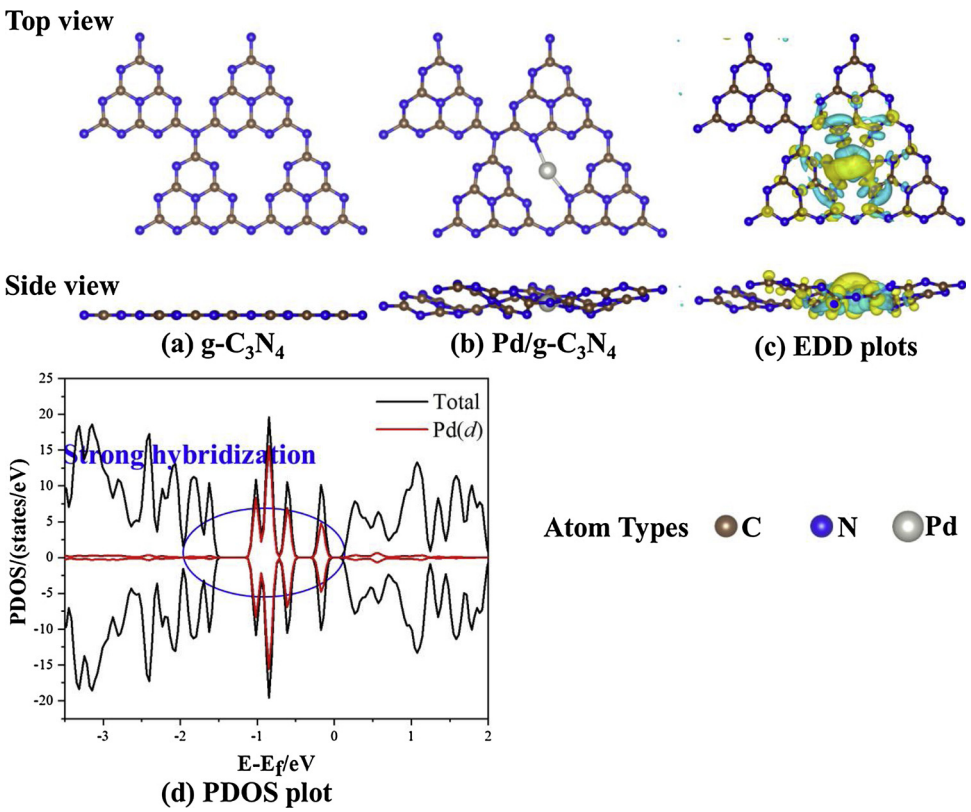

Fig. 1. Structural characteristics of $Pd_{sac}/g\text{-}C_3N_4$ (a) optimized structure of $g\text{-}C_3N_4$ support (b) optimized structure of $Pd_{sac}/g\text{-}C_3N_4$ catalyst (c) electronic density difference (EDD) of catalyst, yellow area represents gaining electrons and cyan-blue area means losing electrons (d) projected density of states (PDOS) of catalyst. (For interpretation of the references to colour in this figure legend, the reader is referred to the web version of this article).

state theory depends on Eq. (6) [74], and the half-life of reactant ($t_{0.5}$) of unimolecular reaction was calculated by Eq. (7) [75].

$$K^{TST} = \frac{K_B T}{h} \times \left(\frac{RT}{P_0}\right)^{\Delta n} \exp\left(\frac{-\Delta G_b}{K_B T}\right) \quad (6)$$

$$t_{0.5} = \ln 2/(K^{TST}) \quad (7)$$

Where K_B is the Boltzmann constant, 8.61×10^{-5} eV·k^{-1} ; T is the Kelvin temperature, K; h is the Planck constant, 6.58×10^{-5} eV·s; ΔG_b is the energy barriers based on Gibbs free energy, eV; $\Delta n = 0$ (unimolecular reaction) or 1 (bimolecular reaction); P_0 represents standard atmosphere pressure (atm), 0.1 MPa.

3. Results and discussions

3.1. The model of $Pd_{sac}/g\text{-}C_3N_4$ catalyst

The optimized structures of $g\text{-}C_3N_4$ support and single-atom palladium catalyst have been provided in the Fig. 1, and some key parameters including average bond length between Pd and N (d, Å), charge transfer on Pd atom (q, e), and binding energy of Pd atom on single-atom catalyst (E_b, eV) were summarized in Table 1, noted that the calculated data in this work kept great consistence with others' research, evidencing our calculation was credible. Stability is a key issue for SACs. He et al. [50] investigated different sites on $g\text{-}C_3N_4$ support, and they found hexagon cavity surrounded by graphitic nitrogen atoms should be the most suitable site to anchor Pd atoms because of the largest binding energy. Li et al. [76] further pointed out single-atom Pd had a high migration energy barrier in this structure. Therefore we constructed model as Fig. 1(b) to simulate $Pd_{sac}/g\text{-}C_3N_4$ in this research. From Fig. 1(c) and Table 1, it was observed that the electrons were running off the metal atom catalyst, so there existed ionic bond effect between metal atom and carbon nitride substrate. In addition, from PDOS plot shown in Fig. 1(d), we discovered a obvious hybrid peak between 4d orbit of Pd atom and $g\text{-}C_3N_4$ carrier, demonstrating strong Pd-N covalent bond formed in catalyst structure. Accordingly, the Pd atom should be anchored stably in the hole of $g\text{-}C_3N_4$ sheet, and the large binding energy of single atom palladium on the surface of $g\text{-}C_3N_4$ might contribute to the combination effect of ionic bond and covalent bond.

Table 1
Key parameters of $Pd_{sac}/g\text{-}C_3N_4$ catalyst, including the average bond length of Pd and N (d, Å), Charge transfer on Pd atom (q,e), and the binding energy of Pd atom on $Pd_{sac}/g\text{-}C_3N_4$ catalyst (E_b,eV).

$Pd/g\text{-}C_3N_4$	$d_{Pd\text{-}N}$(Å)	q_{Pd}(e)	E_b(eV)
Calculated data	2.49	−0.43	−1.43
Literature data	2.49 [76]	−0.50 [77]	−1.42 [76]

3.2. Adsorption characteristic of reaction gases

Adsorption is the origin step of chemical reactions. Moreover, adsorption analysis can offer important guidelines for searching initial and finial structures of reaction paths, so the adsorption characteristics of corresponding gases including a single oxygen atom, oxygen molecule, nitric oxide, nitrogen dioxide, co-adsorption of oxygen with nitric oxide, elemental mercury, and mercuric oxide on the surface of $Pd_{sac}/g\text{-}C_3N_4$ catalyst were studied systematically. Herein, we constructed different adsorption configurations of gases, and selected the most stable adsorption constructions of individual gas molecule, as well as co-adsorption of different reaction gases as research objects as pictured in Fig. 2, with less stable configurations accessible in Fig. S3. In addition, adsorption energy and the bader charge transfer (Δq,e) of substance, Pd atom and adsorbed gases were offered in Table 2. Apparently, adsorbed gas is always being enriched in negative charge (except Hg°), and atomic charge on palladium atom arises from 0.43 e on pure $g\text{-}C_3N_4$ to 0.64 e (O), 0.61 e (O_2), 0.65 e (NO), 0.61 e (NO_2), 0.59 e (NO + O_2), 0.40 e (Hg°, decreasing), 0.69 e (Hg° + O_2), and 0.75 e (HgO), respectively. Considering the electronegativity order of involved elements in

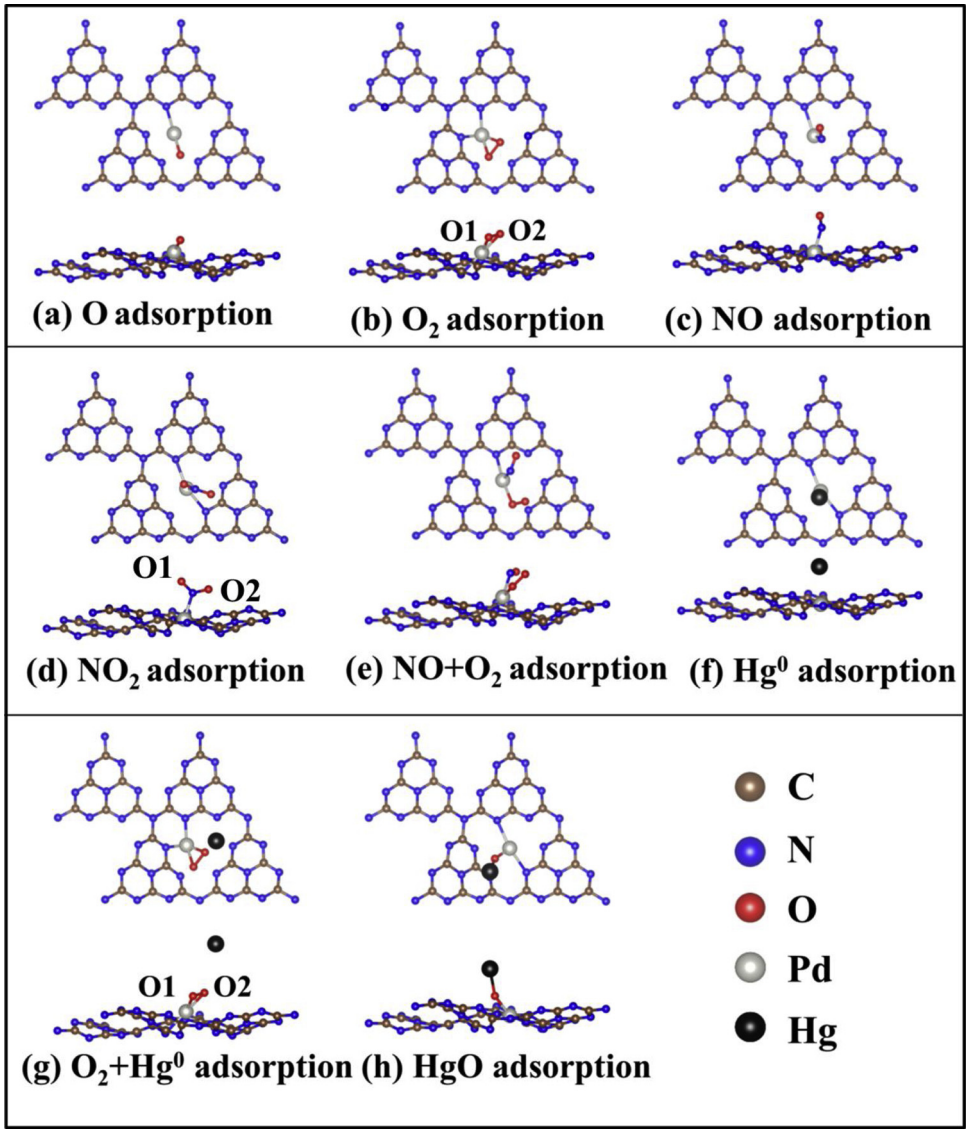

Fig. 2. Adsorption configurations of corresponding reaction gases on $Pd_{sac}/g\text{-}C_3N_4$ catalyst.

Table 2
Bader charge transfer (Δq,e) and adsorption energy (E_{ads}, eV) of reaction gases in adsorption system.

Gas	Δq_{Pd}(e)	$\Delta q_{g\text{-}C3N4}$(e)	Δq_{gas}(e)	E_{ads}(eV)
O	−0.64	0.07	0.57	−3.06(−3.56 [50])
O_2	−0.61	0.25	0.36(0.48 [48])	−0.78(−0.69 [48])
NO	−0.65	0.47	0.18	−1.32
NO_2	−0.61	0.18	0.43	−1.14
NO + O_2	−0.59	0.02	0.57	−1.82
Hg^0	−0.40	0.41	−0.01	−0.30
Hg^0+O_2	−0.69	0.07	0.62	−0.79
HgO	−0.75	0.18	0.57	−1.99

reaction system is O > N > C > Pd > Hg, it is reasonable for Pd atom always transferring electrons to g-C_3N_4 substance as shown in Table 2. Besides, it is because Hg element owns weaker electronegativity than Pd atom, charge transfer of Hg is negative value during adsorption process, which is opposite to other reaction gases.

According to Sabatier principle [78], ideal catalysts should interact with atoms or molecules within a mild strength: interaction between reactants and catalyst should not too weak in order to adsorb the reaction gases, and it also should not too active that may block desorption of products. Oxygen adsorption is the key step of catalytic oxidation and from Table 2, it is found that adsorption energy of oxygen is -0.78 eV, demonstrating this adsorption belongs to chemical adsorption, therefore single-atom Pd catalyst might well has enough activity for catalytic oxidation reactions. In addition, the adsorption energies of NO_2 and HgO are -1.14 eV and -1.99 eV, and these values are obvious lower than reported graphene-supported single-atom iron catalysts with corresponding data of 2.06 eV [66] and 2.34 eV [79], indicating the activity of $Pd_{sac}/g\text{-}C_3N_4$ is within a reasonable interval. Therefore, it is natural and reasonable for us to speculate single-atom Pd catalyst anchoring in g-C_3N_4 carrier may hold potentials on catalytic oxidation of NO and Hg^0.

3.3. Reaction paths of NO oxidation on $Pd_{sac}/g\text{-}C_3N_4$ catalyst

3.3.1. E-R reaction mechanism of NO oxidation

There are two different reaction paths through E-R mechanism in the light of different adsorption configurations of NO molecule attacking adsorbed-state oxygen molecule, and corresponding configurations in reaction steps have been shown in Fig. 3 and Fig. 4. Herein, IS, TS, and FS represent initial state, transition state, and finial state respectively, and virtual frequency values of TS structures were marked

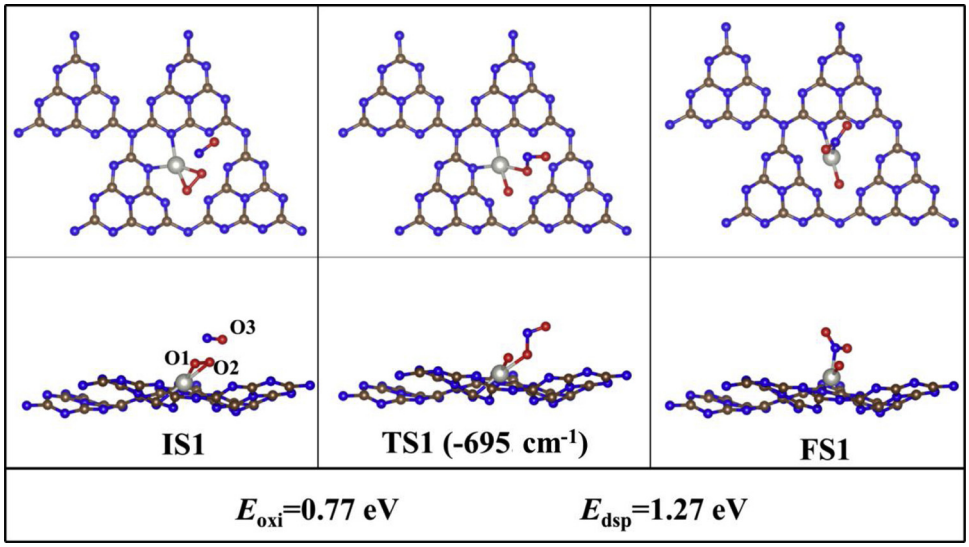

Fig. 3. Top and side views of NO oxidation reaction configurations in E-R mechanism (Path1).

in figures as well. For path1 of E-R mechanism labeled in Fig. 3, the NO molecule firstly adsorbed over the oxygen on the surface of catalyst, and then attacked O2 atom going through 0.77 eV energy barrier to form NO_2 molecule. Given large amounts of literatures have reported that desorption of NO_2 molecule owing high activity tend to be a huge obstacle for recycling of catalysis, it is necessary to take desorption process into consideration when we estimated difficulty of NO catalytic oxidation. In path1 of E-R mechanism, desorption barrier of NO_2 from catalyst surface was 1.27 eV, notice that this value was calculated by subtracting the energy of NO_2 and residual chemical on solid surface (as shown in Fig. 2 (a)) from energy of FS1. Obviously, in this path, the rate-determining step of NO catalytic oxidation is desorption process of product, rather than oxidation generation of NO_2.

Furthermore, we provided a vertical position for NO molecule to interact with adsorbed-state oxygen on catalyst, and the second reaction path was labeled in Fig. 4. Firstly, NO molecule adsorbed over adsorbed-state oxygen with 0.67 eV exothermic heat. Then, the effect of oxygen activation was obvious and played a pivotal role because the bond length of O1-O2 was intensely enlarged from 1.39 Å (IS2) to 1.94 Å (TS2), and then 3.87 Å (FS2) in reaction process. The whole reaction process includes only one transition state, and the oxidation and desorption energy barrier are 1.02 eV and 0.02 eV, respectively. Different from path1 we mentioned above, the rate-determining step of path2 is the oxidation reaction of NO molecule instead of NO_2 desorption. In actual, the reason why NO_2 molecule is hard to escape from catalyst in path1 may well contribute to the existence of an unpaired electron on nitrogen atom according to NO_2 electronic structure, thus making NO_2 molecule more active than some other gases such as CO_2. However, in path2 after formation of adsorption configuration IS2, the oxidation mechanism of NO is the stretching process of O1-O2 bond, and the generated NO_2 molecule would be move away from the active center of catalyst, causing weak desorption energy barrier of NO_2 molecule, so these two reaction paths in E-R mechanism showed different rate-determining steps. Besides two reaction paths we talked above, it is possible that oxygen dissociates with a low activation energy, and then combines with NO in E-R mechanism, however, this reaction mechanism share the same finial state as FS1, demonstrating its rate-determination step is desorption of products. In the view of the whole catalysis reaction process, it is restricted by the same kinetic condition as path1, so we ignore this mechanism in this work.

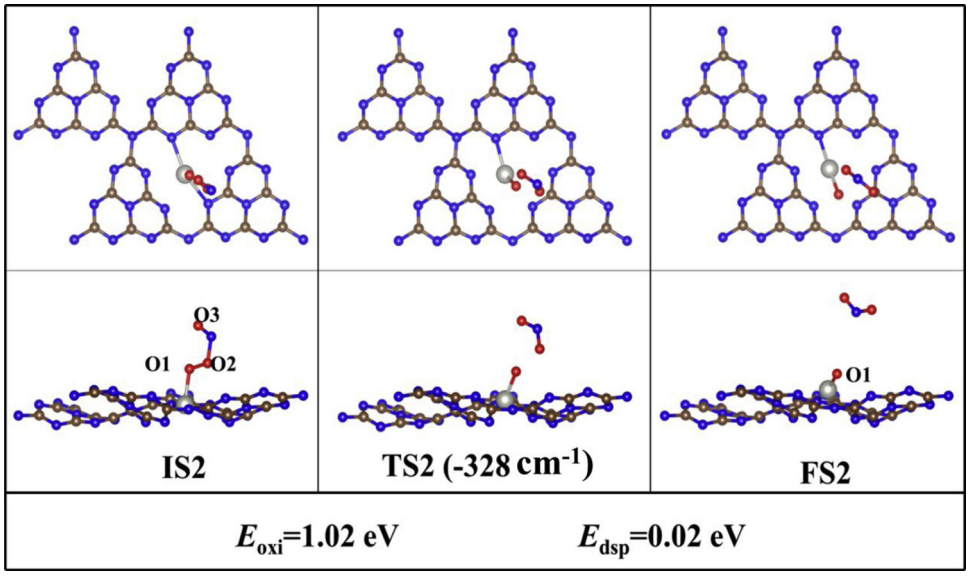

Fig. 4. Top and side views of NO oxidation reaction configurations in E-R mechanism (Path2).

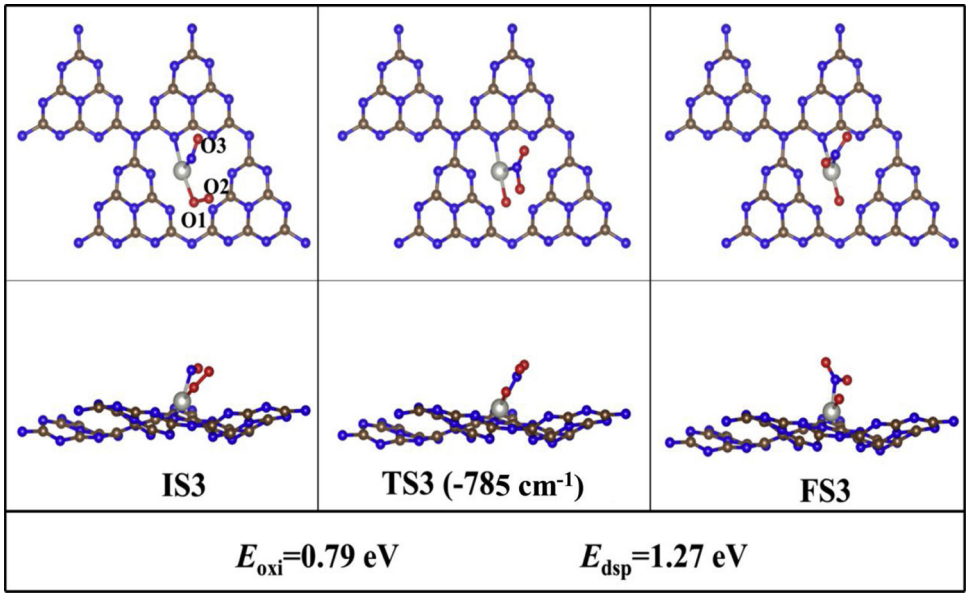

Fig. 5. Top and side views of NO oxidation reaction configurations in L-H mechanism (Path3).

3.3.2. L-H reaction mechanism of NO oxidation

The reaction path of NO oxidation in L-H mechanism was studied and detailed reaction configurations have been shown in Fig. 5. First of all, NO and O_2 bonded on the surface of single-atom catalyst, and in the meanwhile 1.82 eV heat amount was released. The exothermic energy is far more than adsorption energy of oxygen molecule on $Pd_{sac}/g\text{-}C_3N_4$, so in the view of stability of system, the co-adsorption of NO and O_2 in the starting of L-H mechanism would be much more stable compared with single O_2 adsorption in E-R mechanism. After co-adsorption of reactants on catalyst, the O2 atom not directly connected to metal atom gradually took leave from O1 atom, and after getting over the oxidation barrier, O2 atom linked with NO molecule to generate NO_2 molecule. In path3, the oxidation energy barrier from IS3 to FS3 was 0.79 eV, indicating this reaction can happen with ease even at low temperature. In this stage, apparent oxygen activation took place as manifested by bond of lengths of O1-O2 increasing from 1.30 Å (IS3), 1.71 Å(TS3) to 3.32 Å (FS3), so oxygen activation can be seen as one of key indicators in NO oxidation. The desorption energy of NO_2 from FS3 was 1.27 eV, so the chemical reaction rate of NO oxidation in L-H path was determined by desorption process of NO_2, which was very similar to path1 in E-R mechanism.

3.3.3. TER reaction mechanism of NO oxidation

In actual chemical reaction, it is likely that two NO molecules attack oxygen molecule at the same time, and therefore we systematically investigated NO catalytic oxidation by the surface of $Pd_{sac}/g\text{-}C_3N_4$ through TER mechanism, and detailed reaction configurations were plotted in Fig. 6. From IS4 in Fig. 6, we watched that oxygen molecule has been in activated-state, and two NO molecules were attacking oxygen atoms simultaneously above the adsorbed oxidant, and after overcoming a energy barrier of 0.69 eV, the configuration of IS4 was transformed to TS4, and then converted to FS4 where two NO_2 were produced eventually. The oxidation energy barrier through TER mechanism is just 0.69 eV, and this is the lowest value among all reaction paths, indicating NO oxidation can take place with ease by the surface of Pd_{sac}/C_3N_4. It is also implied that even though co-desorption energy barrier of generated two NO_2 reach 1.57 eV, which is the largest desorption barrier among all provided paths, considering symmetry of FS in geometry, if the products escape from the surface of $Pd_{sac}/g\text{-}C_3N_4$ catalyst step by step, the desorption barrier of a single NO_2 molecule should be about 0.79 eV, therefore we speculated the desorption process in TER mechanism would not inhibit catalysis very seriously.

3.3.4. Residual oxygen atom reaction mechanism

Besides TER mechanism, all NO oxidation reactions in E-R mechanism and L-H mechanism consist of two reaction stages. The first stage is NO molecule react with first oxygen atom of oxygen molecule, which has been comprehensively talked about in path1 to path3. The second reaction stage is the removal of residual oxygen atom bonded on the surface of catalyst, whose configuration can be seen in Fig. 2(a), and this stage determines the capacity of catalyst to work continuously.

The removal of residual oxygen is directly related to feasibility of catalysis cycle, because if the energy barrier of removing this oxygen atom is too high, it would seriously hinder the following catalysis reaction. From Table 2, we found the desorption of one oxygen atom need to endothermic 3.06 eV, but the desorption of one NO_2 adsorbed on catalyst just need to take in heat of 1.14 eV, therefore NO catalytic oxidation using residual one oxygen might promote the whole reaction process extremely. Herein, the catalytic oxidation of NO molecule by residual oxygen atom has been provided in Fig. 7, and both energy barrier of NO oxidation and NO_2 desorption were less than 1 eV, suggesting this reaction can take place easily.

3.4. Reaction paths of Hg^0 oxidation on $Pd/g\text{-}C_3N_4$ catalyst

To investigate the feasibility of NO_x and Hg° simultaneous removal by single-atom $Pd/g\text{-}C_3N_4$ catalyst, we furthermore explored Hg° catalytic oxidation. Due to the considerable low volume fraction of mercury species (about 72 μg/L [80]) compared with oxygen (about 4%～6% [81,82]) and NO_x (about 400 ppm [81]) in flue gas, and in the light of the extremely inert of Hg° molecule, we assume it is relatively hard for elemental mercury to compete active sites or co-adsorbed on metal atom catalyst with oxygen molecule. Therefore, L-H and TER mechanism should not be the main reaction mechanism and herein we just talk about possible reaction paths in E-R mechanism.

Reaction configurations of Hg° oxidation in E-R mechanism have been plotted in Fig. 8, and after getting over a energy barrier of 2.09 eV, there exists a structure of O-Hg-O on the surface of catalyst. Even though the oxidation energy barrier of 2.09 eV is relative higher, this mainly results from the selection of weak oxidant (O_2) and the natural inertia caused by full-occupied valence atomic orbit of Hg° as [Ar] $5d^{10}6s^2$. In fact, compared with energy barrier on metal-modified carbonaceous materials (4.27 eV [6]) and V_2O_5/TiO_2 catalyst(more than 5 eV [83]), $Pd_{sac}/g\text{-}C_3N_4$ catalyst owns more outstanding performance on mercury oxidation in the view of catalytic reaction energy barrier.

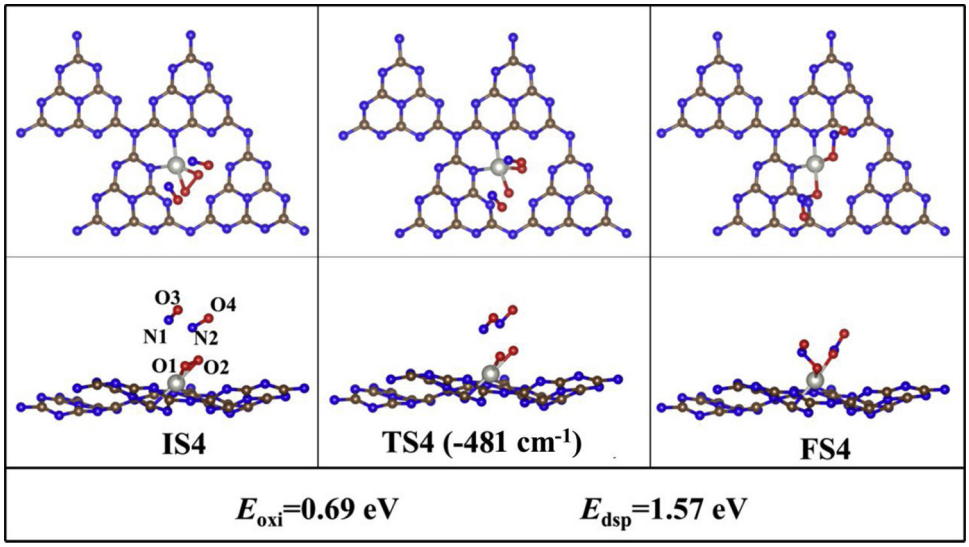

Fig. 6. Top and side views of NO oxidation reaction configurations in TER mechanism (Path4).

Chen et al. [84] studied Hg^0 oxidation by HCl gas on the surface of α-Fe_2O_3, and found the energy barrier was 1.44 eV by DFT calculation, but they ignored the desorption process of generated $HgCl_2$ molecule. In this work, the desorption of newly generated HgO molecule from catalyst surface is a endothermic process with 2.39 eV heat supplement, however in actual, it is just one possibility, because the structure of O-Hg-O is also likely to promote formations of Hg_2O molecule [85], HgO_2 molecule, and Hg_2O_2 cluster [86] in complex flue gas. The generation of HgO_2 is the public stage for four products. In addition, the forming of Hg_2O_2 was considered as Hg^0 adsorption process on FS6, and it was spontaneous, so main products should be determined by desorption barriers. In order to guarantee the comprehensivity of this work, the relative energy variations with different products were talked about and detailed energy changes have been provided in Fig. 9. Given different products and desorption processes, we found the desorption barriers of possible products were 2.39 eV (HgO), 2.17 eV (Hg_2O), 1.84 eV (HgO_2), and 1.81 eV (Hg_2O_2), respectively. Though catalytic oxidation of Hg^0 to different products can take place at the same time, their reaction speeds are varied largely. According to Arenius formula ($k^{TST} = Ae^{-E_a/RT}$), the formation of Hg_2O_2 cluster would exponentially faster than the generation of HgO due to the lowest desorption energy barrier among all possible desorption products. Therefore it will be the dominant mechanism and largely facilitate Hg^0 oxidation. Moreover, if the elemental mercury molecules react with oxygen to yield Hg_2O_2, the issue of residual oxygen atom blocking catalysis cycling would be overcome as well. Thus, the formation of Hg_2O_2 cluster structure would promote the simultaneous removal of nitric oxide and mercury species pollutions using catalytic oxidation method.

3.5. Thermodynamics analysis

We carried out thermodynamic analysis to explore the thermodynamic spontaneity of catalysis reaction. Gibbs free energy variations (ΔG) and the equilibrium constant (K) of different paths were calculated according to Eq. (3). As shown in Fig. 10, most reaction paths of NO oxidation was spontaneous because of $\Delta G < 0$ but reaction pattern regarding to Hg° oxidation could be seen as non-spontaneous process due to $\Delta G > 0$. In detail, the increasing of temperature would strengthen thermodynamics spontaneity in first step of NO oxidation in E-R and L-H mechanisms (path1-path3), but for mechanism of residual oxygen oxidizing NO (path5), the rise of temperature would have an inhibit effect in thermodynamics.

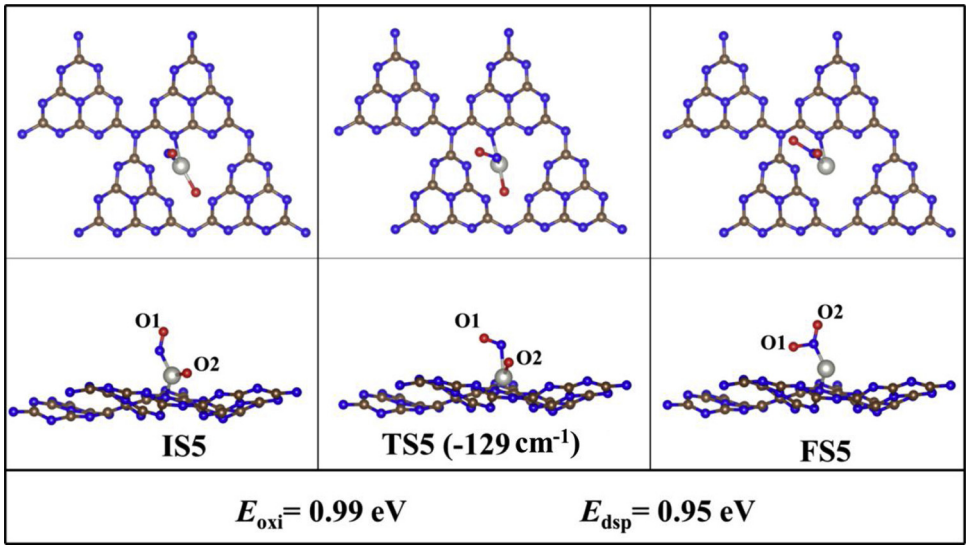

Fig. 7. Top and side views of NO oxidation reaction configurations by residual oxygen (Path5).

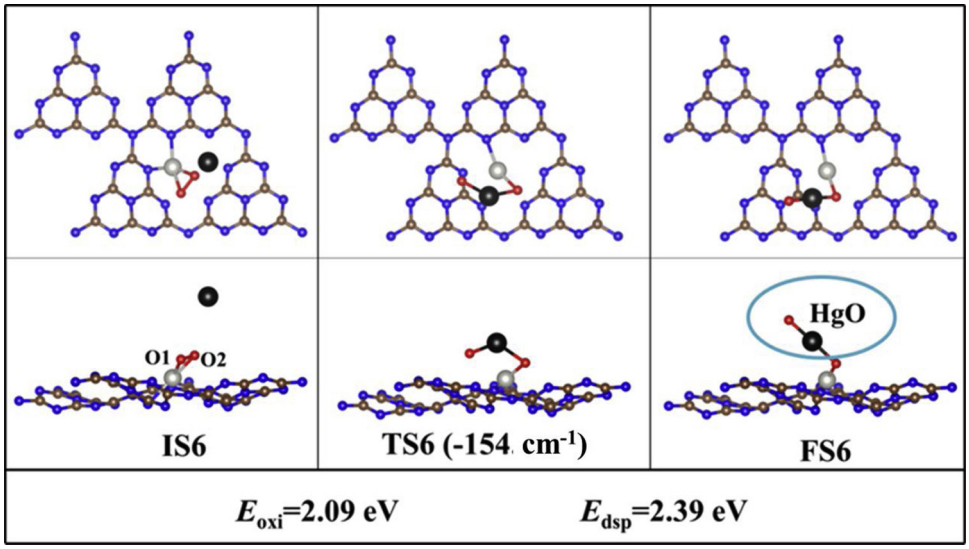

Fig. 8. Top and side views of Hg^0 oxidation reaction configurations in E-R mechanism (Path6).

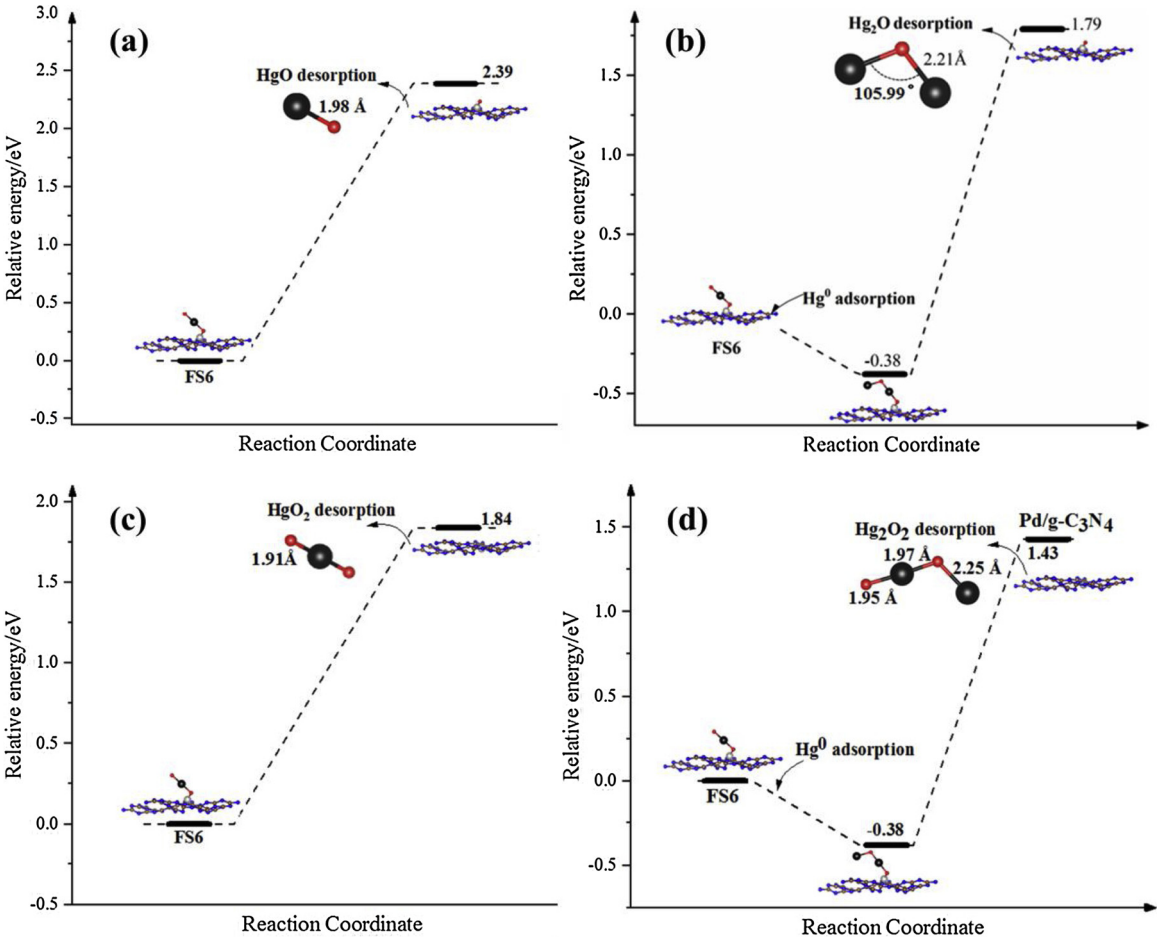

Fig. 9. Different desorption modes of oxides of mercury from FS6 in path6 (a)Directly desorption of HgO molecule from FS6 (b)Formation of Hg_2O_2 cluster and desorption of Hg_2O from FS6 (c)Directly desorption of HgO_2 molecule from FS6 (d)Formation and desorption of Hg_2O_2 cluster from FS6.

From the variations of natural logarithm of equilibrium constants (K) with temperatures exhibited in Fig. 11, we further proved the NO catalytic oxidation by the surface of $Pd_{sac}/g\text{-}C_3N_4$ via path1, path4, and path5 was spontaneous, and this conclusion kept agreement with above analysis about ΔG. Moreover, when temperature was under 650 K, equilibrium constants was more than 10^5, evidencing the conversion rate of forward direction of NO oxidation will be far deeper than that of reverse direction and those reaction steps can take place completely and irreversibly. Besides, the values of $\Delta G < 0$ and K in path3 was smaller than 10^5, suggesting NO oxidation by L-H mechanism was spontaneous, but the chemical reaction depth was not very well, so the reactants can hardly be converted to NO_2 completely. As for path2, it was observed

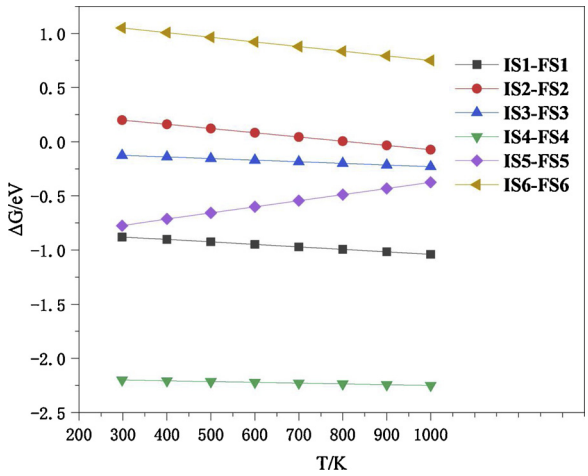

Fig. 10. Gibbs free energy variations of different reaction paths with different temperatures.

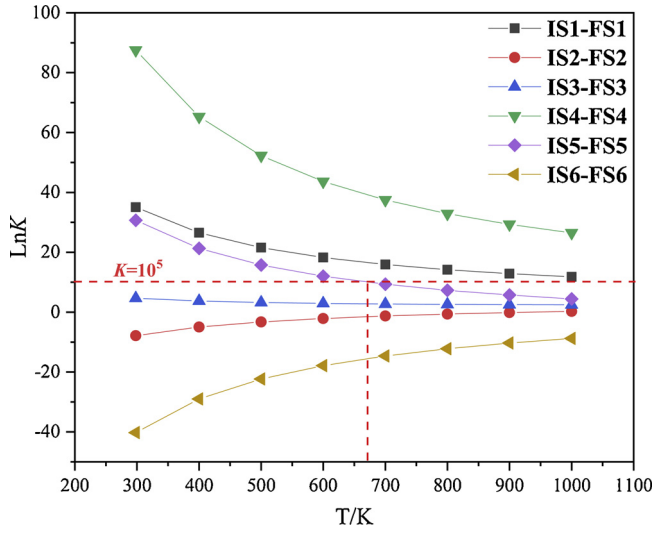

Fig. 11. Natural logarithm of equilibrium constants (K) with different temperatures.

that both path1 and path2 belonged to E-R reaction mechanism, but different from path1, path2 was a non-spontaneous reaction, however, considering the fact that IS1 was more stable than IS2 owing to higher adsorption energy, we can conclude the occurrence possibility of path1 was far more than that of path2 in E-R mechanism, so path2 would not the main NO catalytic oxidation path in E-R mechanism. In the light of the fact that $\Delta G > 0$ and $\mathrm{Ln}K < 0$, Hg° oxidation on the surface of Pd_{sac}/g-C_3N_4 was always non-spontaneous reaction. Some studied Hg° oxidation on the surface of RuO_2/TiO_2 [20] and V_2O_5/TiO_2 catalysts [87] respectively, and they found FS structures in reaction paths tended to have higher relative energy than IS or other stable intermediates, indicating catalytic oxidation of Hg° always need continuous endothermic devotion, which kept great consistence with the conclusion in this work.

3.6. Kinetic analysis

In flue gas, the possibility of trimolecular reactions is far less than that of unimolecular reactions and bimolecular reactions. In addition, the contents of Hg and NO is just about 0.72 μg/L and 400 ppm in flue gas, leading to it is very hard for two Hg or NO molecules attacking adsorbed-state oxygen at the same time, so the TER mechanism of catalytic oxidation was ignored in kinetic analysis. For IS1 in path1 as

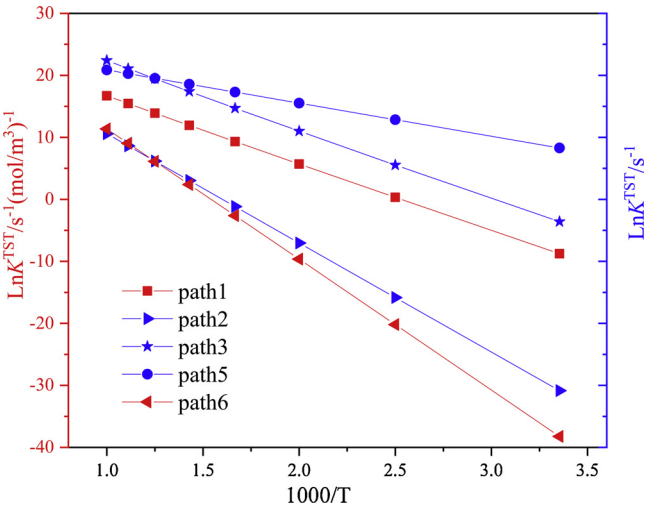

Fig. 12. Natural logarithm of reaction rate constants (K^{TST}) of oxidation reaction step with different temperatures.

well as IS6 in path6, we can consider oxygen and catalyst as a whole due to stable chemical adsorption of oxygen on Pd_{sac}/g-C_3N_4. Then we calculate the adsorption energy of NO molecule and Hg° over the adsorption system (O_2 + catalyst) is 0.41 eV and 0.02 eV, respectively, both not belonging to chemical adsorption. Moreover, from Fig. 3, we can also observe NO molecule do not bind on adsorbed oxygen strongly, further suggesting NO molecule interact with adsorbed oxygen weakly. Therefore the small interactions between NO and catalyst containing oxygen suggest IS1 and IS6 are unstable and reactants can hardly form stable intermediate complexes, and the reaction modes of path1 and path6 are bimolecular reactions. In contrast, for the IS2, IS3 and IS5, all reactants have been connected on Pd_{sac}/C_3N_4 inseparable in geometry, and the adsorption energy of all reactants on Pd_{sac}/C_3N_4 catalyst are up to -1.10 eV, -1.82 eV and -3.07 eV, so we consider path2, path3 and path6 should belong to unimolecular reactions.

Natural logarithms of reaction rate constants (K^{TST}) of oxidation reaction step have been plotted in Fig. 12, and we observe high temperature can greatly promote the chemical reaction rate. To intuitively reveal chemical reaction speed, we further provided half-life of reactants ($t_{0.5}$) for unimolecular reaction in Table S2, and it has been found that the conversion of reactants is very spanking even at low temperature, for example the $t_{0.5}$ of NO oxidation by L-H mechanism (path3) is less than 0.007 hour at room temperature (298.15 K, 1 atm). Moreover, we find the $t_{0.5}$ of reactants in residual oxygen removal process (path5) is only 4.87×10^{-8} hour at low temperature (298.15 K, 1 atm), indicating Pd_{sac}/g-C_3N_4 barely suffer from the issue of residual oxygen atom poisoning which seriously block catalytic activity of some other carbonaceous catalysts [66,88]. According to Arrhenius formula, we fit out the prefactor (A) and activation energy (E_a) in Table 3, and the result demonstrates that catalytic oxidation of NO and Hg° by the surface of Pd_{sac}/g-C_3N_4 catalyst can take place easily, and the activation energy are 0.46 eV and 1.81 eV, respectively.

The desorption barriers of NO_2 are 0.02 eV ~ 1.57 eV in this work and these values are far less than that of single vacancy graphene-based

Table 3
kinetic parameters for different reaction paths.

Paths	E_a/eV	A
Path1-NO oxidation	0.93	$8.09 \times 10^{11}/s^{-1}(mol/m^3)^{-1}$
Path2-NO oxidation	1.52	$1.73 \times 10^{12}/s^{-1}$
Path3-NO oxidation	0.95	$2.15 \times 10^{14}/s^{-1}$
Path5-NO oxidation	0.46	$2.39 \times 10^{11}/s^{-1}$
Path6-Hg^0 oxidation	1.81	$1.26 \times 10^{14}/s^{-1}(mol/m^3)^{-1}$

single-atom iron catalyst (2.06 eV [66]) we reported previously. In the meanwhile, Hg^{2+} desorption would not a serious issue because compared activation energy of Hg^0, the desorption energy of Hg_2O_2 (1.81 eV) is not very large. In the light of large oxidation rate by kinetic analysis and the relative desorption energy barriers of products, we confirmed that $Pd_{sac}/g\text{-}C_3N_4$ can be a potential catalyst for oxidation removal of NO and Hg^0.

4. Conclusions

In this work, we systematically study the adsorption mechanism and catalytic oxidation patterns of NO and Hg° on the surface of $g\text{-}C_3N_4$-based single-atom palladium catalyst. The detailed reaction modes in L-H, E-R and TER mechanism are researched. In addition, corresponding thermodynamic and kinetic analysis have been carried out to obtain the temperature effect on the equilibrium constant and reaction rate. It is found that most of reaction paths are spontaneous, and for NO catalytic oxidation, almost all equilibrium constants exceed 10^5, suggesting reactions of NO oxidation are irreversible. Kinetic analysis reveals that half-life of reactants is very short, and the lowest activation energies of NO and Hg° oxidation are just 0.46 eV and 1.81 eV, respectively. Considering the advantages of outstanding activity, high utilization rate of metal atoms, and avoiding usage of toxic oxidant, we conclude that $Pd_{sac}/g\text{-}C_3N_4$ catalyst can be a potential material for catalytic oxidation removal of NO and Hg°.

CRediT authorship contribution statement

Xiaoshuo Liu: Conceptualization, Methodology, Formal analysis, Writing - original draft. **Zhengyang Gao:** Resources, Supervision, Project administration, Funding acquisition. **Hanyu Huang:** Data curation, Investigation. **Ge Yan:** Visualization. **Tianfang Huang:** Validation. **Cong Chen:** Software. **Weijie Yang:** Writing - review & editing, Funding acquisition. **Xun-Lei Ding:** Writing - review & editing, Funding acquisition.

Declaration of Competing Interest

There are no conflicts to declare.

Acknowledgement

This work was supported by National Natural Science Foundation of China (No. 91545122), Beijing Natural Science Foundation (2182066), Natural Science Foundation of Hebei Province of China (B2018502067), and the Fundamental Research Funds for the Central Universities (JB2015RCY03 and 2017XS121). That all computational results depend on Tian-He2 super computer at Lvliang should be acknowledged.

Appendix A. Supplementary data

Supplementary material related to this article can be found, in the online version, at doi:https://doi.org/10.1016/j.mcat.2020.110901.

References

[1] D. Liu, D. Chen, N. Li, Q. Xu, H. Li, J. He, et al., Integration of 3D macroscopic graphene aerogel with 0D-2D $AgVO_3$-$g\text{-}C_3N_4$ heterojunction for highly efficient photocatalytic oxidation of nitric oxide, Appl. Catal. B 243 (2019) 576–584.
[2] S. Zhao, D. Pudasainee, Y. Duan, R. Gupta, M. Liu, J. Lu, A review on mercury in coal combustion process: Content and occurrence forms in coal, transformation, sampling methods, emission and control technologies, Prog. Energy Combust. Sci. 73 (2019) 26–64.
[3] C. Chen, Y. Cao, S. Liu, J. Chen, W. Jia, The catalytic properties of Cu modified attapulgite in NH_3–SCO and NH_3–SCR reactions, Appl. Surf. Sci. 480 (2019) 537–547.
[4] H. Tang, W. You, Z. Wang, C. Li, C. Zhu, L. Cai, et al., Detrimental effects of SO_2 on gaseous mercury(II) adsorption and retention by CaO-based sorbent traps: competition and heterogeneous reduction, J. Hazard. Mater. 387 (2020) 121679.
[5] W. Yang, Z. Gao, X. Liu, X. Ding, W. Yan, The adsorption characteristics of As_2O_3, Pb°, PbO and $PbCl_2$ on single atom iron adsorbent with graphene-based substrates, Chem. Eng. J. 361 (2019) 304–313.
[6] X. Liu, Z. Gao, C. Wang, M. Zhao, X. Ding, W. Yang, et al., Hg^0 oxidation and SO_3, Pb^0, PbO, $PbCl_2$ and As_2O_3 adsorption by graphene-based bimetallic catalyst ((Fe,Co)@N-GN): a DFT study, Appl. Surf. Sci. 496 (2019).
[7] J. Liu, X. Shi, Y. Shan, Z. Yan, W. Shan, Y. Yu, et al., Hydrothermal stability of CeO_2–WO_3–ZrO_2 mixed oxides for selective catalytic reduction of NO_x by NH_3, Environ. Sci. Technol. 52 (20) (2018) 11769–11777.
[8] C. Liu, F. Li, J. Wu, X. Hou, W. Huang, Y. Zhang, et al., A comparative study of MO_x (M = Mn, Co and Cu) modifications over $CePO_4$ catalysts for selective catalytic reduction of NO with NH_3, J. Hazard. Mater. 363 (2019) 439–446.
[9] L. Zhao, C. Li, S. Li, Y. Wang, J. Zhang, T. Wang, et al., Simultaneous removal of elemental mercury and NO in simulated flue gas over V_2O_5/ZrO_2-CeO_2 catalyst, Appl. Catal. B 198 (2016) 420–430.
[10] L. Zhong, Y. Zhang, Y. Ji, P. Norris, W.-P. Pan, Calorimetry. Synthesis of activated carbon from coal pitch for mercury removal in coal-fired power plants, J. Therm. Anal. 123 (1) (2016) 851–860.
[11] F. Shen, J. Liu, Y. Dong, D. Wu, Mercury removal by biomass-derived porous carbon: experimental and theoretical insights into the effect of H_2S, Chem. Eng. J. 348 (2018) 409–415.
[12] W. Qu, J. Liu, F. Shen, P. Wei, Y. Lei, Mechanism of mercury-iodine species binding on carbonaceous surface: insight from density functional theory study, Chem. Eng. J. 306 (2016) 704–708.
[13] S. Cui, Z. Zhong, Y. Liao, L. Qi, D. Fu, Simultaneous removal of NO and SO_2 via an integrated system of nonthermal plasma combined with catalytic oxidation and wet electrostatic precipitator, Energy Fuels 33 (10) (2019) 10078–10089.
[14] Y. Liu, Y. Wang, Q. Wang, J. Pan, J. Zhang, Simultaneous removal of NO and SO_2 using vacuum ultraviolet light (VUV)/heat/peroxymonosulfate (PMS), Chemosphere 190 (2018) 431–441.
[15] X.-L. Duan, C.-G. Yuan, T.-T. Jing, X.-D. Yuan, Removal of elemental mercury using large surface area micro-porous corn cob activated carbon by zinc chloride activation, Fuel 239 (2019) 830–840.
[16] M.S. Maqbool, A.K. Pullur, H.P. Ha, Novel sulfation effect on low-temperature activity enhancement of CeO_2-added Sb-V_2O_5/TiO_2 catalyst for NH_3-SCR, Appl. Catal. B 152 (2014) 28–37.
[17] Z. Hong, Z. Wang, X. Li, Catalytic oxidation of nitric oxide (NO) over different catalysts: an overview, Catal. Sci. Technol. 7 (16) (2017) 3440–3452.
[18] Yu Y-k, C. He, Chen J-s, X.-r. Meng, Deactivation mechanism of de-NO_x catalyst (V_2O_5-WO_3/TiO_2) used in coal fired power plant, J. Fuel Chem. Technol. 40 (11) (2012) 1359–1365.
[19] C. Liu, L. Chen, J. Li, L. Ma, H. Arandiyan, Y. Du, et al., Enhancement of activity and sulfur resistance of CeO_2 supported on TiO_2–SiO_2 for the selective catalytic reduction of NO by NH_3, Environ. Sci. Technol. 46 (11) (2012) 6182–6189.
[20] Y. Yang, J. Liu, Z. Wang, S. Miao, J. Ding, Y. Yu, et al., A complete catalytic reaction scheme for Hg(0) oxidation by HCl over RuO_2/TiO_2 catalyst, J. Hazard. Mater. 373 (2019) 660–670.
[21] B. Yang, A. Peng, X. Wang, Q. Huang, M. Chen, Y. Shen, et al., Simultaneous catalytic oxidation of CO and Hg° over Au/TiO_2 catalysts: structure and mechanism study, Mol. Catal. 479 (2019) 110633.
[22] H. Wang, B. Yuan, R. Hao, Y. Zhao, X. Wang, A critical review on the method of simultaneous removal of multi-air-pollutant in flue gas, Chem. Eng. J. 378 (2019).
[23] Y. Ling, C. Zhang, J. Wu, W. Xu, Y. Qi, P. He, et al., Enhanced photocatalytic activity of TiO_2 by micrometer-scale flower-like morphology for gaseous elemental mercury removal, Catal. Commun. 116 (2018) 91–95.
[24] Y. Guan, J. Wu, Q. Liu, M. Gu, Y. Lin, Y. Qi, et al., Fabrication of BiOI/MoS_2 heterojunction photocatalyst with different treatment methods for enhancing photocatalytic performance under visible-light, Mater. Res. Bull. 120 (2019) 110579.
[25] Z. Liu, F. Yu, C. Ma, J. Dan, J. Luo, B. Dai, A critical review of recent progress and perspective in practical denitration application, Catalysts 9 (9) (2019) 771.
[26] Z. Wang, J. Liu, Y. Yang, F. Liu, J. Ding, Heterogeneous reaction mechanism of elemental mercury oxidation by oxygen species over MnO_2 catalyst, Proceedings of the Combustion Institute 37 (2019), pp. 2967–2975 3.
[27] S. Cui, R. Hao, D. Fu, Integrated method of non-thermal plasma combined with catalytical oxidation for simultaneous removal of SO_2 and NO, Fuel 246 (2019) 365–374.
[28] Y. Chen, X. Guo, F. Wu, Y. Huang, Z. Yin, Experimental and theoretical studies for the mechanism of mercury oxidation over chlorine and cupric impregnated activated carbon, Appl. Surf. Sci. 458 (2018) 790–799.
[29] A.A. Presto, E.J. Granite, Survey of catalysts for oxidation of mercury in flue gas, Environ. Sci. Technol. 40 (18) (2006) 5601–5609.
[30] Z. Wang, J. Liu, B. Zhang, Y. Yang, Z. Zhang, S. Miao, Mechanism of heterogeneous mercury oxidation by HBr over V_2O_5/TiO_2 catalyst, Environ. Sci. Technol. 50 (10) (2016) 5398–5404.
[31] Z. Wen, Z. Wang, Y. Li, K. Cen, Mechanism and kinetic study on elemental mercury oxidation in flue gas by ozone injection, Ozone Sci. Eng. 40 (1) (2018) 29–36.
[32] Z. Gao, S. Lv, W. Yang, P. Yang, S. Ji, X. Meng, Quantum chemistry investigation on the reaction mechanism of the elemental mercury, chlorine, bromine and ozone system, J. Mol. Model. 21 (6) (2015) 160.
[33] X. Gao, Z. Du, Ding H-l, Wu Z-l, H. Lu, Luo Z-y, et al., Kinetics of NO_x absorption into $(NH4)_2SO_3$ solution in an ammonia-based wet flue gas desulfurization process, Energy Fuels 24 (11) (2010) 5876–5882.
[34] J. Liu, M.A. Cheney, F. Wu, M. Li, Effects of chemical functional groups on elemental mercury adsorption on carbonaceous surfaces, J. Hazard. Mater. 186 (1)

(2011) 108–113.
[35] Z. Gao, X. Liu, A. Li, C. Ma, X. Li, X. Ding, et al., Adsorption behavior of mercuric oxide clusters on activated carbon and the effect of SO_2 on this adsorption: a theoretical investigation, J. Mol. Model. 25 (5) (2019).
[36] H. Wang, S. Wang, Y. Duan, Li Y-n, Z. Ying, Experimental study of homogeneous Hg oxidation in air and oxy-simulated flue gas, J. Energy Inst. 92 (2) (2019) 257–264.
[37] H. Kamata, Ueno S-i, N. Sato, T. Naito, Mercury oxidation by hydrochloric acid over TiO_2 supported metal oxide catalysts in coal combustion flue gas, Fuel Process. Technol. 90 (7–8) (2009) 947–951.
[38] B. Yang, Z. Li, Q. Huang, M. Chen, L. Xu, Y. Shen, et al., Synergetic removal of elemental mercury and NO over TiCe0.25Sn0.25Ox catalysts from flue gas: performance and mechanism study, Chem. Eng. J. 360 (2019) 990–1002.
[39] Z. Gao, X. Liu, A. Li, X. Li, X. Ding, W. Yang, Bimetallic sites supported on N-doped graphene ((Fe, Co)/N-GN) as a new catalyst for NO oxidation: a theoretical investigation, Mol. Catal. 470 (2019) 56–66.
[40] L. Zhao, C. Li, X. Zhang, G. Zeng, J. Zhang, Y. Xie, A review on oxidation of elemental mercury from coal-fired flue gas with selective catalytic reduction catalysts, Catal. Sci. Technol. 5 (7) (2015) 3459–3472.
[41] W. Hou, J. Zhou, C. Yu, S. You, X. Gao, Z. Luo, et al., Pd/Al_2O_3 sorbents for elemental mercury capture at high temperatures in syngas, Ind. Eng. Chem. Res. 53 (23) (2014) 9909–9914.
[42] G. Xu, R. Wang, F. Yang, D. Ma, Z. Yang, Z. Lu, CO oxidation on single Pd atom embedded defect-graphene via a new termolecular Eley-Rideal mechanism, Carbon 118 (2017) 35–42.
[43] Y. Wang, J. Mao, X. Meng, L. Yu, D. Deng, X. Bao, Catalysis with two-dimensional materials confining single atoms: concept, design, and applications, Chem. Rev. 119 (3) (2019) 1806–1854.
[44] S. Liang, C. Hao, Y. Shi, The power of single-atom catalysis, ChemCatChem 7 (17) (2015) 2559–2567.
[45] D. Deng, K.S. Novoselov, Q. Fu, N. Zheng, Z. Tian, X. Bao, Catalysis with two-dimensional materials and their heterostructures, Nat. Nanotechnol. 11 (3) (2016) 218–230.
[46] S. Phalinyot, C. Tabtimsai, B. Wanno, Nitrogen monoxide storage and sensing applications of transition metal–doped boron nitride nanotubes: a DFT investigation, Struct. Chem. 30 (6) (2019) 2135–2149.
[47] E. Vorobyeva, Z. Chen, S. Mitchell, R.K. Leary, P. Midgley, J.M. Thomas, et al., Tailoring the framework composition of carbon nitride to improve the catalytic efficiency of the stabilised palladium atoms, J. Mater. Chem. A 5 (31) (2017) 16393–16403.
[48] Y. Rao, X. Duan, Pd/Pt embedded CN monolayers as efficient catalysts for CO oxidation, J. Chem. Soc. Faraday Trans. 21 (46) (2019) 25743–25748.
[49] G. Gao, Y. Jiao, E.R. Waclawik, A. Du, Single atom (Pd/Pt) supported on graphitic carbon nitride as an efficient photocatalyst for visible-light reduction of carbon dioxide, J. Am. Chem. Soc. 138 (19) (2016) 6292–6297.
[50] F. He, K. Li, C. Yin, Y. Wang, H. Tang, Z. Wu, Single Pd atoms supported by graphitic carbon nitride, a potential oxygen reduction reaction catalyst from theoretical perspective, Carbon 114 (2017) 619–627.
[51] M.C. Payne, M.P. Teter, D.C. Allan, T. Arias, a J. Joannopoulos, Iterative minimization techniques for ab initio total-energy calculations: molecular dynamics and conjugate gradients, Rev. Mod. Phys. 64 (4) (1992) 1045.
[52] Z. Feng, Y. Tang, W. Chen, D. Wei, Y. Ma, X. Dai, O-doped graphdiyne as metal-free catalysts for nitrogen reduction reaction, Mol. Catal. 483 (2020) 110705.
[53] R. Zhang, L. Jiao, W. Yang, G. Wan, H.-L. Jiang, Single-atom catalysts templated by metal–organic frameworks for electrochemical nitrogen reduction, J. Mater. Chem. A 46 (7) (2019) 26371–26377.
[54] Z. Gao, Y. Sun, M. Li, W. Yang, X. Ding, Adsorption sensitivity of Fe decorated different graphene supports toward toxic gas molecules (CO and NO), Appl. Surf. Sci. 456 (2018) 351–359.
[55] A.D. Becke, E.R. Johnson, Exchange-hole dipole moment and the dispersion interaction, J. Chem. Phys. 122 (15) (2005) 154104.
[56] S. Grimme, J. Antony, S. Ehrlich, H. Krieg, A consistent and accurate ab initio parametrization of density functional dispersion correction (DFT-D) for the 94 elements H-Pu, J. Chem. Phys. 132 (15) (2010) 154104.
[57] S. Liu, L. Chen, X. Mu, M. Xu, J. Yu, G. Yang, et al., Development of $Pd_n/g\text{-}C_3N_4$ adsorbent for Hg^0 removal – DFT study of influences of the support and Pd cluster size, Fuel 254 (2019).
[58] P. Li, F. Wang, S. Wei, X. Li, Y. Zhou, Mechanistic insights into CO_2 reduction on Cu/Mo-loaded two-dimensional $g\text{-}C_3N_4(001)$, Phys. Chem. Chem. Phys. 19 (6) (2017) 4405–4410.
[59] Z. Liu, D. Zhang, T. Wei, L. Wang, X. Li, B. Liu, Adsorption characteristics of formaldehyde on nitrogen doped graphene-based single atom adsorbents: a DFT study, Appl. Surf. Sci. 493 (2019) 1260–1267.
[60] Z. Gao, A. Li, X. Li, X. Liu, C. Ma, J. Yang, et al., The adsorption and activation of oxygen molecule on nickel clusters doped graphene-based support by DFT, Mol. Catal. 477 (2019) 110547.
[61] Z. Gao, X. Li, A. Li, C. Ma, X. Liu, J. Yang, et al., Adsorption behavior of Pt embedded on N-doped graphene sheets toward NO and NH3 molecules, Appl. Organomet. Chem. 33 (9) (2019) e5079.
[62] H. Li, Z. Zhang, Z. Liu, Non-monotonic trends of hydrogen adsorption on single atom doped $g\text{-}C_3N_4$, Catalysts 9 (1) (2019) 84.
[63] G. Henkelman, H. Jónsson, Improved tangent estimate in the nudged elastic band method for finding minimum energy paths and saddle points, J. Chem. Phys. 113 (22) (2000) 9978–9985.
[64] G. Henkelman, B.P. Uberuaga, H. Jónsson, A climbing image nudged elastic band method for finding saddle points and minimum energy paths, J. Chem. Phys. 113 (22) (2000) 9901–9904.
[65] A. Heyden, A.T. Bell, F.J. Keil, Efficient methods for finding transition states in chemical reactions: comparison of improved dimer method and partitioned rational function optimization method, J. Chem. Phys. 123 (22) (2005) 224101.
[66] W. Yang, Z. Gao, X. Liu, X. Li, X. Ding, W. Yan, Single-atom iron catalyst with single-vacancy graphene-based substrate as a novel catalyst for NO oxidation: a theoretical study, Catal. Sci. Technol. 8 (16) (2018) 4159–4168.
[67] W. Yang, Z. Gao, X. Liu, C. Ma, X. Ding, W. Yan, Directly catalytic reduction of NO without NH_3 by single atom iron catalyst: a DFT calculation, Fuel 243 (2019) 262–270.
[68] C. Riplinger, E.A. Carter, Cooperative effects in water binding to cuprous oxide surfaces, J. Phys. Chem. C 119 (17) (2015) 9311–9323.
[69] P. He, J. Wu, X. Jiang, W. Pan, J. Ren, Effect of SO_3 on elemental mercury adsorption on a carbonaceous surface, Appl. Surf. Sci. 258 (22) (2012) 8853–8860.
[70] P. He, X. Zhang, X. Peng, X. Jiang, J. Wu, N. Chen, Interaction of elemental mercury with defective carbonaceous cluster, J. Hazard. Mater. 300 (2015) 289–297.
[71] Z. Gao, G. Yan, M. Zhao, S. Xu, L. Li, H. Huang, et al., Theoretical insights into the stability of perovskite clusters by studying water adsorption on $(CH3NH_3)_4SnI_6$, Sol. Energy Mater. Sol. Cells 202 (2019) 110126.
[72] P.A. Korevaar, S.J. George, A.J. Markvoort, M.M. Smulders, P.A. Hilbers, A.P. Schenning, et al., Pathway complexity in supramolecular polymerization, Nature 481 (7382) (2012) 492.
[73] C. Ling, L. Shi, Y. Ouyang, X.C. Zeng, J. Wang, Nanosheet supported single-metal atom bifunctional catalyst for overall water splitting, Nano Lett. 17 (8) (2017) 5133–5139.
[74] G. Bravo-Pérez, J.R. Alvarez-Idaboy, A. Cruz-Torres, M.E. Ruíz, Quantum chemical and conventional transition-state theory calculations of rate constants for the NO3+ alkane reaction, J. Phys. Chem. A 106 (18) (2002) 4645–4650.
[75] < https://chem.libretexts.org/Bookshelves/Physical_and_Theoretical_Chemistry_Textbook_Maps/Supplemental_Modules_(Physical_and_Theoretical_Chemistry)/Kinetics/Reaction_Rates/Half-lives_and_Pharmacokinetics > .
[76] H. Li, Y. Wu, L. Li, Y. Gong, L. Niu, X. Liu, et al., Adjustable photocatalytic ability of monolayer $g\text{-}C_3N_4$ utilizing single–metal atom: density functional theory, Appl. Surf. Sci. 457 (2018) 735–744.
[77] S.L. Li, H. Yin, X. Kan, L.Y. Gan, U. Schwingenschlogl, Y. Zhao, Potential of transition metal atoms embedded in buckled monolayer $g\text{-}C_3N_4$ as single-atom catalysts, Phys. Chem. Chem. Phys. 19 (44) (2017) 30069–30077.
[78] A.J. Medford, A. Vojvodic, J.S. Hummelshøj, J. Voss, F. Abild-Pedersen, F. Studt, et al., From the Sabatier principle to a predictive theory of transition-metal heterogeneous catalysis, J. Catal. 328 (2015) 36–42.
[79] W. Yang, L. Linlin, M. Zhao, H. Huang, X. Ding, C. Wu, et al., Theoretical prediction of graphene-based single-atom iron as a novel catalyst for catalytic oxidation of Hg^0 by O_2, Appl. Surf. Sci. 508 (2020) 145035.
[80] C. Chen, W. Jia, S. Liu, Y. Cao, Simultaneous NO removal and Hg^0 oxidation over CuO doped $V_2O_5\text{-}WO_3/TiO_2$ catalysts in simulated coal-fired flue gas, Energy Fuels 32 (6) (2018) 7025–7034.
[81] S. Zhang, Y. Zhao, Z. Wang, J. Zhang, L. Wang, C. Zheng, Integrated removal of NO and mercury from coal combustion flue gas using manganese oxides supported on TiO_2, J. Environ. Sci. (China) 53 (2017) 141–150.
[82] Z. Wei, S. Yu, Z. Huang, X. Xiao, M. Tang, B. Li, et al., Simultaneous removal of elemental mercury and NO by mercury induced thermophilic community in membrane biofilm reactor, Ecotoxicol. Environ. Saf. 176 (2019) 170–177.
[83] Y. Gao, Z. Li, Y. Hao, Effect of M-Doped (M = Cr, Fe, Co, and Nb) $V_2O_5/TiO_2(001)$ on mercury oxidation: the insights from DFT calculation, J. Phys. Chem. C 121 (50) (2017) 27963–27975.
[84] Y. Chen, X. Guo, F. Wu, Y. Huang, Z. Yin, Mechanisms of mercury transformation over $\alpha\text{-}Fe_2O_3$ (0 0 1) in the presence of HCl and/or H_2S, Fuel 233 (2018) 309–316.
[85] J. Zhang, Y. Duan, W. Zhao, C. Zhu, Q. Zhou, M. She, Removal of elemental mercury from simulated flue gas by combining non-thermal plasma with calcium oxide, Plasma Chem. Plasma Process. 36 (2) (2015) 471–485.
[86] C. Wang, S. Xu, Y. Cui, Optical and bonding characters of Hg type clusters, New J. Chem. 37 (10) (2013) 3303–3307.
[87] Wu Y-w, Z. Ali, Q. Lu, J. Liu, Xu M-x, L. Zhao, et al., Effect of WO_3 doping on the mechanism of mercury oxidation by HCl over V_2O_5/TiO_2 (001) surface: periodic density functional theory study, Appl. Surf. Sci. 487 (2019) 369–378.
[88] Z. Gao, W. Yang, X. Ding, Y. Ding, W. Yan, Theoretical research on heterogeneous reduction of N_2O by char, Appl. Therm. Eng. 126 (2017) 28–36.